International Journal of Mechanical Sciences 83 (2014) 146–154

Contents lists available at ScienceDirect

International Journal of Mechanical Sciences

journal homepage: www.elsevier.com/locate/ijmecsci

Fracture in hole-flanging produced by single point incremental forming

V.A. Cristino [a], L. Montanari [b], M.B. Silva [c], A.G. Atkins [d], P.A.F. Martins [c,*]

[a] Department of Electromechanical Engineering, University of Macau, Av. Padre Tomás Pereira Taipa, Macau, China
[b] Escola de Engenharia de São Carlos, University of São Paulo, Av. Trabalhador São-Carlense, 400, São Carlos, CEP: 13566-590, Brazil
[c] Instituto Superior Tecnico, Universidade de Lisboa, Av. Rovisco Pais, 1049-001 Lisboa, Portugal
[d] Department of Engineering, University of Reading, Box 225, Reading RG6 6AY, UK

ARTICLE INFO

Article history:
Received 19 November 2013
Received in revised form
6 March 2014
Accepted 1 April 2014
Available online 5 April 2014

Keywords:
Incremental sheet forming
Hole-flanging
Plasticity
Ductile damage
Fracture toughness

ABSTRACT

Hole flanging produced by single point incremental forming is a new manufacturing process in which a sheet, with a concentric pre-cut hole and the outer periphery rigidly fixed by a blank holder, is progressively forced with a tool to produce cylindrical or conical smooth flanges. The formability limits of the process are known to be higher than those commonly found in hole-flanging produced by conventional press-working due to suppression of necking with a low growth rate of accumulated strains above the forming limit curve.

The aim and objectives of the paper is to evaluate the critical values of fracture toughness and ductile damage at crack initiation according to different damage laws and to correlate these values with independently determined values of the forming limits at fracture. The presentation starts by tracing the strains and stresses of various positions over the surface of the hole-flanged parts at different intermediate stages of deformation. It is revealed that the strain loading ratios are constant for different material elements. From these data, the experimental values of accumulated damage at various positions are determined, particularly at the site of fracture.

1. Introduction

Single Point Incremental Forming (SPIF) is a dieless manufacturing process that progressively shapes a blank (clamped rigidly around its edges, but unsupported underneath) by means of a simple hemispherical-ended forming tool that may be free or rotating and which describes the contour of the desired geometry. Fig. 1 presents the basic components of the process: (a) the sheet metal blank, (b) the rig with the backing plate, (c) the pressure pad, and (d) the rotating single-point forming tool.

In the early years of development of SPIF most studies concerned experimental investigations on the capability and flexibility of the process to produce prototypes and small batches of sheet metal parts (Fig. 1a) in which the path of the rotating tool was driven by either ordinary computer numerical control machine tools or special purpose machine tools. Only a limited number of studies on the characterization of the formability limits of the process in terms of the major operative variables have been carried out in this period. The keynote paper by Jeswiet et al. [1] provides a comprehensive review of the research on SPIF that was performed between the end of 1990s and 2005.

The understanding of the deformation mechanics of SPIF and of the physics behind failure just came recently by means of finite element studies [2,3], analytical developments [4,5], experimental measurements and observations [6,7]. Typical modes of deformation were identified, different mechanisms to explain plastic deformation above the forming limit curve (FLC) were proposed and the formability limits of the process were established across the useful range of process conditions. The state-of-the-art review paper by Emmens and van den Boogaard [8] presents an overview of the most significant contributions in the field with special emphasis on the mechanisms that were proposed to explain plastic deformation above the FLC.

The focus on the above mentioned mechanisms was due to experimental observation that failure in SPIF occurred by thinning without evidence of localized necking taking place before reaching the onset of fracture. The first explanation of plastic flow above the FLC in the light of modern ductile fracture mechanics was proposed by Silva et al. [4] who employed a ductile damage criterion based on the triaxiality ratio $\sigma_m/\overline{\sigma}$ between the hydrostatic stress σ_m and the effective (flow) stress $\overline{\sigma}$ to determine the slope of the fracture forming line (FFL) in the principal strain space. The prediction of the formability limits of SPIF by means of

* Corresponding author.
E-mail address: pmartins@ist.utl.pt (P.A.F. Martins).

http://dx.doi.org/10.1016/j.ijmecsci.2014.04.001
0020-7403/

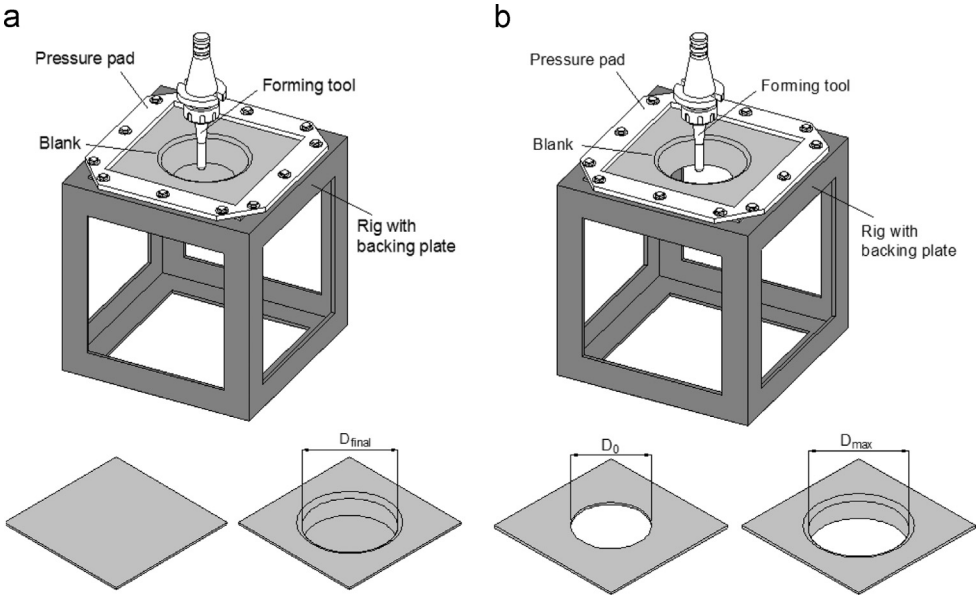

Fig. 1. Schematic representation of the fabrication of (a) sheet metal parts and (b) flanges in sheet metal blanks with pre-cut holes by means of SPIF.

ductile damage criteria was further investigated by other researchers. Cao et al. [5], for example, combined the Oyane ductile fracture criterion [9] with an analytical model to quantitatively understand the effects of tooling and process parameters related to sheet thickness. Huang et al. [10] produced finite element estimates of the onset of fracture in a conical cup by means of the Oyane ductile fracture criterion. Malhotra et al. [11] made use of the plasticity damage model due to Xue [12] and performed finite element analysis of a cone and a funnel with a plasticity damage criterion to demonstrate that the local nature of deformation in SPIF and suppression of necking is primarily responsible for the increased formability, in spite of greater damage accumulation as compared to conventional press-working.

The abovementioned methodologies to correlate ductile damage and plastic flow above the FLC made use of different procedures to determine the critical values of damage. Silva et al. [4], for example, measured the strains of a SPIF benchmark sheet metal part at the onset of failure to set up critical damage and the position of the FFL in the principal strain space. Cao et al. [5] measured the strains at the onset of failure in two different types of tensile tests to determine the material constants of the Oyane ductile damage criterion. Huang et al. [10] utilized a similar procedure to that of Cao et al. [5] with data retrieved from bi-axial tensile tests available in the literature. Malhotra et al. [11] performed a manual adjustment of the different constants of Xue's ductile damage material model by matching the forming tool z-forces obtained from finite element simulation with those measured during the experiments.

None of the above mentioned publications presents a simple, effective and independent methodology to determine the critical values of damage at crack initiation directly from the experimental values of strains and stresses at various positions over the spiffed workpieces. Moreover, nobody has ever considered the possibility of determining fracture toughness of sheet metal products by means of SPIF.

In fact, the successful determination of the critical values of damage and fracture toughness at crack initiation are among the most relevant experimental data to be supplied to finite element computer programs that are commonly utilized to simulate sheet metal forming and single point incremental forming, in particular.

Under these circumstances, the aim and objective of this paper is to combine circle-grid analysis due to Keeler [13] and Goodwin [14] and failure map concepts due to Glover et al. [15] to trace strains and stresses along the deformation history of material and determine the experimental values of critical damage and fracture toughness. Experiments in hole-flanging produced by SPIF (Fig. 1b) give support to the presentation.

The organization of the paper is the following. Section 2 summarizes the procedures utilized in mechanical and formability characterization of the material, presents the essentials of the new proposed methodology to determine the critical values of damage and fracture toughness, and describes the work plan utilized in background hole-flanging experiments. Section 3 presents and discusses the results, analyzing plastic flow above the FLC in the light of the FFL, ductile damage and fracture toughness. Section 4 presents the conclusions.

2. Material and methods

2.1. Mechanical and formability characterization

The research work was carried out on aluminum AA1050-H111 sheets with 1 mm thickness. The specimens utilized in the mechanical and formability characterization of the material were cut out from the supplied sheets at 0°, 45° and 90° degrees with respect to the rolling direction.

The mechanical characterization of the material was performed by means of tensile tests in an Instron 4507 testing machine and the average stress–strain curve was approximated by the following Ludwik–Hollomon's equation:

$$\sigma = 140\varepsilon^{0.04}\ (\text{MPa}) \tag{1}$$

The values obtained for the modulus of elasticity E, the yield strength σ_Y, the ultimate tensile strength σ_{UTS}, the anisotropy coefficient r and the elongation at break A at 0°, 45° and 90° degrees with respect to the rolling direction are provided in Table 1. The average value of the anisotropy coefficient $\bar{r}$ is obtained from,

$$\bar{r} = \frac{r_0 + 2r_{45} + r_{90}}{4} \tag{2}$$

The formability limits at necking (FLC) and fracture (FFL) were characterized by means of laboratory formability tests that cover strain paths from uniaxial to plane-strain and biaxial loading conditions. The technique utilized for measuring the in-plane

Table 1
Summary of the mechanical properties of the aluminum AA1050-H111 sheets that were utilized in the investigation.

	Modulus of elasticity ***E*** **(GPa)**	**Yield strength** σ_Y **(MPa)**	**Ultimate tensile strength** σ_{UTS} **(MPa)**	**Anisotropy coefficient** ***r***	**Elongation at break** ***A*** **(%)**
0° RD	72.7	115.4	119.0	0.71	7.1
45° RD	67.9	120.4	121.2	0.88	5.2
90° RD	71.8	123.0	120.8	0.87	5.6
Average	70.0	119.9	120.5	0.84	6.8

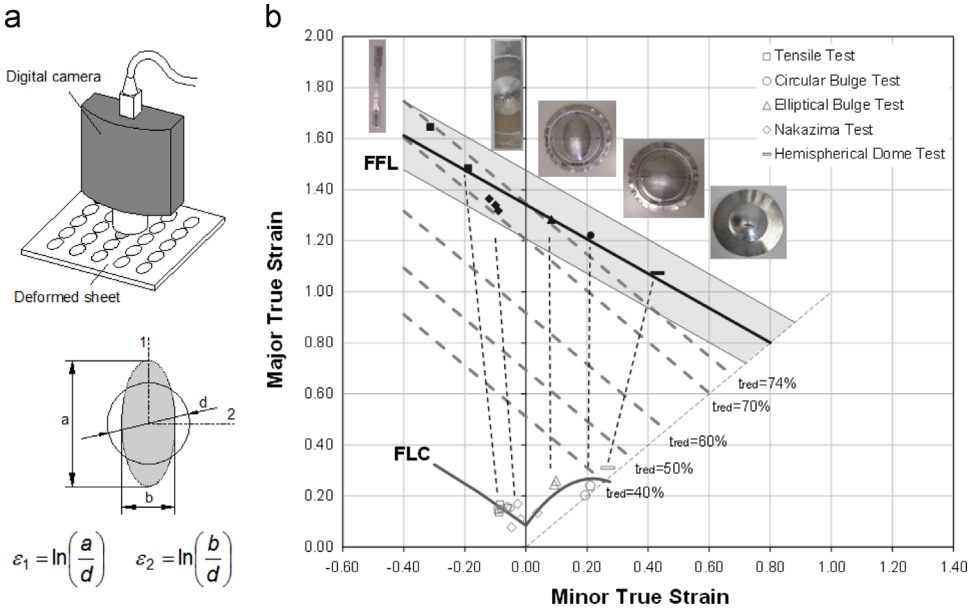

Fig. 2. Formability limits of aluminum AA1050-H111 built upon a wide range of experimental tests. (a) Schematic representation of the procedure utilized for measuring the major and minor in-plane strains that resulted from plastic deformation of the circles during sheet formability tests. (b) Forming limit curve (FLC), fracture forming limit (FFL) and several iso-thickness reduction lines in the principal strain space. The solid markers refer to failure by fracture and the black dotted lines show the change in strain path direction towards plane strain after necking.

strains (ε_1, ε_2) and obtaining the FLC involved electrochemical etching of a grid of overlapping circles with 2 mm initial diameter on the surface of the test specimens before forming and measuring the major and minor axis of the ellipses that resulted from the plastic deformation of the circles during the tests, by means of a computer-aided measuring system (CAMS) (Fig. 2a).

The FFL was determined by measuring the thickness before and after fracture at several locations along the crack in order to obtain the 'gauge length' strains. The resulting formability limits at necking (FLC) and fracture (FFL) are plotted in Fig. 2b and the gray area around the FFL corresponds to an uncertainty of 10% in its determination. The iso-thickness reduction lines $t_{red}\,(\%) = 100 \times (t_0 - t)/t_0$ where, t_0 and t are the original (undeformed) and the actual sheet thickness, were determined from the condition of constant thickness strain at fracture [16],

$$t_{red}(\%) = 100 \times (1 + \exp^{\varepsilon_1 + \varepsilon_2}) \tag{3}$$

As seen in Fig. 2b, the reduction in sheet thickness at the onset of fracture corresponds to maximum values $t_{red} > 70\%$.

Further details on the experimental techniques that were employed to determine the FLC and the FFL can be found elsewhere [7].

2.2. Methodology for determination of the critical damage and fracture toughness

The proposed methodology for determining critical damage and fracture toughness extends the isotropic conditions assumed by Glover et al. [15] in their work on failure maps in sheet metal forming and traces the deformation history of material elements in SPIF according to the procedure that was recently proposed by Montanari et al. [17] in order to determine the energy per volume and the specific work of surface formation at the onset of fracture under anisotropic plastic flow.

Under these circumstances and taking into consideration that strain loading paths of hole-flanged parts produced by SPIF remain proportional during the deformation history of material elements (refer to Section 3), the evaluation of strains, stresses and damage will be performed under the assumption of linear strain-paths with a slope β defined as,

$$\beta = \frac{d\varepsilon_2}{d\varepsilon_1} = \frac{\varepsilon_2}{\varepsilon_1} \tag{4}$$

The in-plane strains ε_1 and ε_2 in (4) are measured from the major and minor axis of the ellipses that result from the plastic deformation of the circles during the hole-flanging experiments (refer to the schematic representation of the procedure in Fig. 2a).

Assuming that the average value of the anisotropy coefficient $\bar{r}$ is constant during straining and considering the anisotropic yield criterion due to Hill [18] under plane stress conditions $\sigma_3 = 0$, the associated flow rule relating the in-plane strain increments with the applied stresses is expressed as (in what follows $\bar{r}$ will be simply written as r),

$$d\varepsilon_1 = \frac{d\bar{\varepsilon}}{\bar{\sigma}}\left[\frac{1}{1+r}\right](\sigma_1 + r(\sigma_1 - \sigma_2))$$

$$d\varepsilon_2 = \frac{d\bar{\varepsilon}}{\bar{\sigma}}\left[\frac{1}{1+r}\right](\sigma_2 + r(\sigma_2 - \sigma_1)) \tag{5}$$

where the effective strain increment $d\bar{\varepsilon}$ and the effective stress $\bar{\sigma}$ are respectively calculated from,

$$d\bar{\varepsilon} = \frac{1+r}{\sqrt{(1+2r)}}\sqrt{d\varepsilon_1^2 + d\varepsilon_2^2 + \frac{2r}{(1+r)}d\varepsilon_1\, d\varepsilon_2} \tag{6}$$

and,

$$\bar{\sigma} = \sqrt{\sigma_1^2 + \sigma_2^2 - \frac{2r}{(1+r)}\sigma_1\sigma_2} \tag{7}$$

Now, determining the ratio $d\varepsilon_2/d\varepsilon_1$ between the minor and major strain increments (5) and assuming proportional loading conditions with a slope $\alpha = \sigma_2/\sigma_1$, one obtains,

$$\alpha = \frac{\sigma_2}{\sigma_1} = \frac{(1+r)\beta + r}{(1+r) + r\beta} \tag{8}$$

By replacing (8) into (7), the following expressions for the principal in-plane stresses σ_1 and σ_2 are obtained,

$$\sigma_1 = \frac{\bar{\sigma}}{\sqrt{\left(1 - \frac{2r}{1+r}\alpha + \alpha^2\right)}} \quad \sigma_2 = \frac{\alpha\bar{\sigma}}{\sqrt{\left(1 - \frac{2r}{1+r}\alpha + \alpha^2\right)}} \tag{9}$$

where $\bar{\sigma}$ is calculated from the stress–strain curve of the material (1) after integrating the increment of effective strain $d\bar{\varepsilon}$ up to the current plastic deformation $\bar{\varepsilon} = \int d\bar{\varepsilon}$.

The proposed methodology for determining critical damage considers that fracture is triggered when a damage function D reaches a critical value. Therefore, once the values of strains and stresses have been obtained for the entire deformation paths (strain and stress paths) of the sheet metal part, it is possible to obtain the critical value of damage D^{crit} by integrating the damage function D at the location of crack initiation from beginning until the onset of failure.

The presentation makes use of two ductile fracture criteria based on the triaxiality ratio $\sigma_m/\bar{\sigma}$ that was originally proposed by McClintock and is known to play an important role in the formability of materials [16]. The damage functions D associated with the ductile fracture criteria proposed by Ayada et al. [19] and Rice and Tracey [20], take the form,

$$D_{Ayada} = \int_0^{\bar{\varepsilon}} \frac{\sigma_m}{\bar{\sigma}} d\bar{\varepsilon}$$

$$D_{Rice-Tracey} = \int_0^{\bar{\varepsilon}} \exp\left(\frac{3}{2} \times \frac{\sigma_m}{\bar{\sigma}}\right) d\bar{\varepsilon} \tag{10}$$

where σ_m is the average stress and $\bar{\varepsilon}$ is the effective strain at a specific location. In case of a location corresponding to crack initiation, the effective strain $\bar{\varepsilon} = \bar{\varepsilon}_f$ and the accumulated values of damage given by (10) become the critical values of damage (D^{crit}_{Ayada} and $D^{crit}_{Rice-Tracey}$) at the onset of failure.

The overall investigation could have been easily extended to other ductile fracture criteria available in the literature [21] but the application of the proposed methodology for determination of the critical damage would basically remain identical.

The proposed methodology for determining fracture toughness at the location of crack initiation considers plastic work that makes up the specific work of fracture (the fracture toughness, R) to be dissipated in thin boundary layers alongside the crack surfaces (Fig. 3). Such work is given by the plastic work/volume up to the effective strain at fracture $\bar{\varepsilon}_f$ multiplied by the volume of the boundary layer, as proposed by Atkins and Mai [22]. For an increase in crack area dA, the associated volume increase is hdA where h is the thickness of the boundary layer and the associated plastic work W is,

$$W = \left(\int_0^{\bar{\varepsilon}_f} \bar{\sigma}\, d\bar{\varepsilon}\right) h\, dA \tag{11}$$

Because fracture toughness R is defined as the plastic work given by Eq. (11) divided by the increase in crack area, it follows that,

$$R \cong t \int_0^{\bar{\varepsilon}_f} \bar{\sigma}\, d\bar{\varepsilon} \tag{12}$$

where the thickness of the boundary layer h is taken as the thickness t of the deformed sheet. This approximation copes with Atkins and Mai [23] and is justified by the fact that hole-flanging produced by multi-stage SPIF gives rise to a significant and uniform reduction of the initial thickness t_0 of the sheet (sometimes above 70%) and, therefore, it is reasonable to assume that the boundary layer h alongside the crack surface is of the order of magnitude of the thickness t of the deformed sheet.

The results of the proposed methodology will be discussed in Section 3.

2.3. Background experiments

The experiments in hole-flanging produced by multi-stage SPIF were performed with aluminum AA1050-H111 blanks with 250 mm × 250 mm × 1 mm. The blanks were drilled at the center to deliver holes with two different diameters D_0 and subsequently ground with medium and fine grit sand paper to eliminate burrs, cracks and to make the edges perpendicular to the surfaces. After

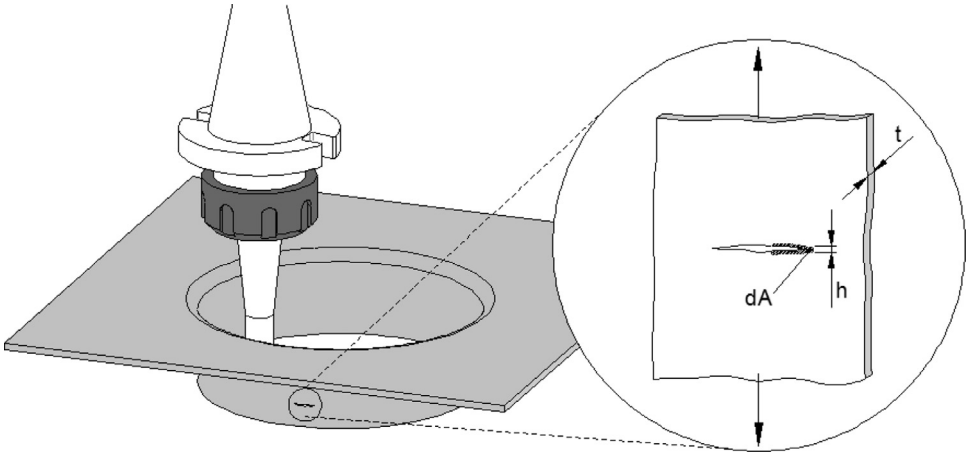

Fig. 3. Terminology utilized in the procedure for determining fracture toughness at crack initiation. The hatched region denotes the thin boundary layers alongside the crack.

Table 2
Experimental work plan for the hole-flanging tests produced by SPIF.

(Pre-cut) Hole diameter D_0 (mm)	Tool diameter (mm)	Drawing angle of the intermediate stages ψ_i (°)					
		1st	2nd	3rd	4th	5th	6th
121	8	65	70	75	80	85	90
102							

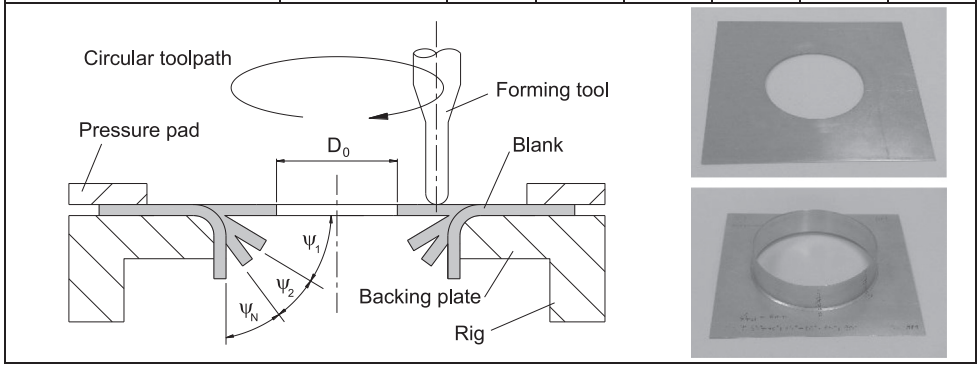

being ground, the blanks were electrochemically-etched with grids of circles of 2.5 mm in diameter in order to allow in-plane strains to be measured from the deformed ellipses. The flanges were shaped by means of a multi-stage forward tool path strategy that made use of progressively increasing drawing angles from $\psi_1 = 65^\circ$, until $\psi_6 = 90^\circ$ with steps of $\Delta\psi = 5^\circ$ (Table 2).

The forming tool had a hemispherical tip with 8 mm diameter and was made from cold working 120WV4-DIN tool steel, hardened and tempered to 60 HRc. The tests were performed with helical tool paths characterized by a step size per revolution equal to 0.2 mm (downward feed) and a feed rate equal to 1000 mm/min. The rotation of the forming tool was free.

3. Results and discussion

3.1. Strains and stresses

The deformation history of hole-flanging produced by multi-stage SPIF was characterized by tracing the strain paths of selected grid points (A–J) located along the meridional direction of the blanks at different intermediate stages of deformation (refer to the intermediate drawing angles in Table 2 and Fig. 4a).

In case of blanks with a pre-cut hole diameter $D_0 = 121$ mm, the strain paths of points A–J at the six intermediate drawing angles ($\psi_i = 65$–90°) grow linearly and monotonically from the origin to the maximum achievable strains (refer to the thin black lines in Fig. 4a). In other words, there are no changes in the strain paths at the transition from the FLC towards the FFL in contrast to what was previously observed for tensile, bi-axial circular and elliptical bulge formability tests, which experience a change in direction towards vertical plane strain conditions, (refer to the black dotted lines in Fig. 2).

The thick black curve in Fig. 4a is the envelope of the greatest achievable strains for any linear strain path in hole-flanging produced by SPIF and will be hereafter referred as 'the strain envelope'. The points (I, J) located near the hole edge undergo equal biaxial stretching, the points (F–H) located at the transition region between the flange wall and the hole edge evolve under biaxial stretching, and the points located at the corner (A, B) and at the flange wall (C–E) experience near plane-strain conditions.

The shape of the envelope clearly indicates the critical region, where strains are larger and closer to the FFL, to be located at the flange wall (refer to points C–E) and not at the hole edge as it is commonly found in hole-flanging by conventional press-working. This is because the material placed at the vicinity of the hole edge deforms under biaxial stretching ($d\varepsilon_\phi, d\varepsilon_\theta > 0$) instead of uniaxial tension (as in case of hole-flanging by conventional press-working) due to combination of plane strain deformation ($d\varepsilon_\phi : d\varepsilon_\theta : d\varepsilon_t = 1 : 0 : -1$) typical of incremental sheet metal forming and uniaxial tension ($d\varepsilon_\phi : d\varepsilon_\theta : d\varepsilon_t = -1/2 : 1 : -1/2$) associated with the progressive increase of the inner diameter of the hole.

The stress paths, the stress envelope corresponding to the greatest achievable stresses and the locus of the stress states corresponding to the FLC and the FFL are plotted in Fig. 4b and were determined by means of Eq. (8).

The analysis of both Fig. 4a and b allows concluding that point C is the closest to failure but still allowed the fabrication of a sound sheet metal part from a hole-flanged blank with a pre-cut hole diameter $D_0 = 121$ mm.

3.2. Ductile damage

Fig. 5 presents contours of accumulated damage as a function of the experimental in-plane strains (ε_1, ε_2). Two damage functions are considered: Ayada's (Fig. 5a) and Rice–Tracey's (Fig. 5b).

As seen in the figures, the contours of accumulated damage appear as a family of inclined lines failing from left to right with a slope similar to that of the experimentally determined FFL. The grid point C, located at the mid of the flange wall and undergoing near plane strain loading conditions, experiences the greatest values of accumulated damage $D^{max}_{Ayada} = 0.75$ and $D^{max}_{Rice-Tracey} = 3.12$. Conversely, the grid point J located near the hole edge and undergoing equal biaxial stretching experiences the lowest values of accumulated damage. This result explains the reason why failure by cracking in hole-flanged parts made from blanks with pre-cut hole diameters $D_0 = 102$ mm will take place at the flange walls (around point C) and not at the hole edges.

The black dashed lines corresponding to the iso-accumulated damage loci in Fig. 5 were plotted after rewriting Eq. (10) as a function of the strain ratio β.

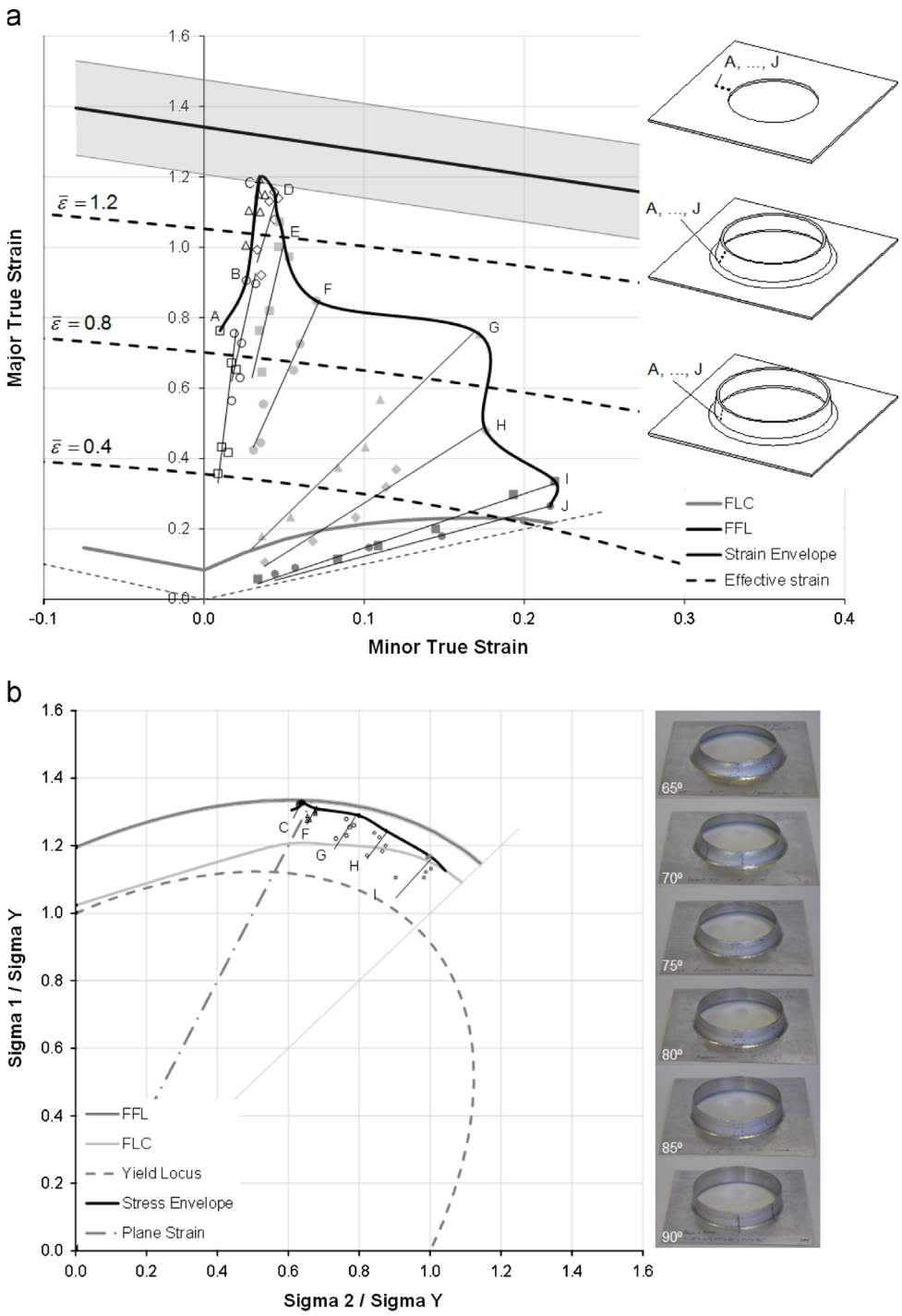

Fig. 4. Deformation history of the grid points A to J located along the meridional direction of a hole-flanged sheet metal part with a pre-cut hole diameter $D_0 = 121$ mm at drawing angles $\psi_i = 65–90°$. (a) Representation of the strain paths in the principal strain space. The black curve is the strain envelope and the dashed black elliptical curves are iso-effective strain contours. (b) Representation of the stress paths in the principal stress space. The black curve is the stress envelope. Note: The axis of the principal stress space are normalized to the yield stress σ_Y, the dashed gray elliptical curves refer to the yield locus and the dashed-dotted gray line corresponds to plane strain.

Taking into consideration that point C undergoes plastic deformation along near-plane strain conditions (that is, along a proportional strain-path with a slope $\beta \approx 0$) and bearing in mind that the ratio $\sigma_m/\overline{\sigma}$ of the damage functions D in Eq. (10) is constant along the strain loading path, it is possible to obtain the greatest accumulated value of damage directly from the experimental measurement of the maximum effective strain $\overline{\varepsilon}^{max}$ located in the strain envelope (refer to the elliptical dashed black curves corresponding to the iso-effective strain contours in Fig. 4a). This possibility requires writing the average stress σ_m and the effective stress $\overline{\sigma}$ (7) under a proportional plane strain loading path $\beta = 0$, as follows,

$$\sigma_m = \frac{1+2r}{3(1+r)}\sigma_1 \quad \overline{\sigma} = \frac{\sqrt{1+2r}}{(1+r)}\sigma_1 \tag{13}$$

and replacing (13) into the damage functions D (10), in order to obtain,

$$D^{max}_{Ayada} = \frac{1}{3}\sqrt{1+2r}\,\overline{\varepsilon}^{max}$$

$$D^{max}_{Rice-Tracey} = \exp\left(\frac{1}{2}\sqrt{1+2r}\right)\overline{\varepsilon}^{max} \tag{14}$$

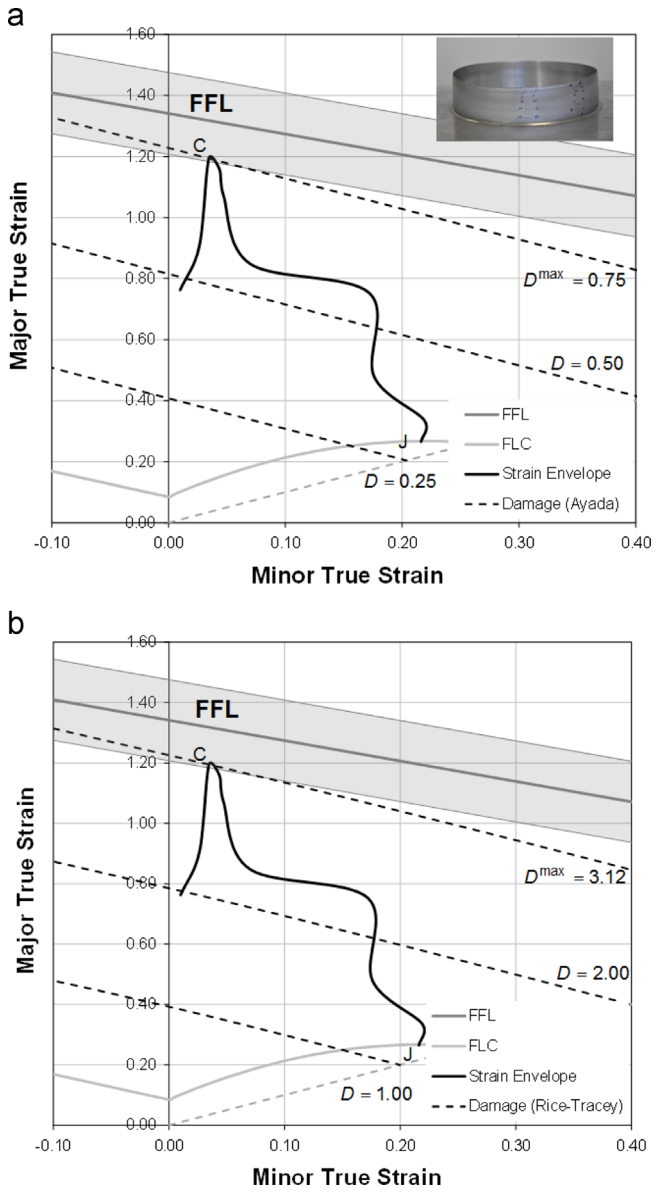

Fig. 5. Strain envelope in the principal strain space with line contours (black dashed lines) showing different values of accumulated damage D according to (a) Ayada et al. and (b) Rice and Tracey for a hole-flanged part made from a blank with a pre-cut hole diameter $D_0 = 121$ mm.

The above equations provide a simple and effective procedure to obtain the maximum accumulated damage D^{max} at the wall flange without the necessity of integrating the damage functions D along the strain loading paths. The values determined by Eq. (14) can be taken as approximations of the critical values of damage D^{crit} at crack initiation provided by means of Eq. (10), if the observed cracks are assumed to be triggered under plane strain deformation conditions.

Considering, for example, point C (Fig. 5) located at the surface of the hole-flanged part produced from a blank with a pre-cut hole diameter $D_0 = 121$ mm and experiencing a maximum effective strain $\bar{\varepsilon}^{max} = 1.36$, it is possible to estimate approximate values of the maximum accumulated damage (14) as $D^{max}_{Ayada} = 0.74$ and $D^{max}_{Rice-Tracey} = 3.08$. These values are in good agreement with the iso-accumulated contours of damage $D^{max}_{Ayada} = 0.75$ and $D^{max}_{Rice-Tracey} = 3.12$ plotted in Fig. 5, which were obtained by integrating the damage functions along the strain paths by means of Eq. (10).

The small differences found in the results provided by the two above mentioned methodologies are explained by the fact that point C experiences near-plane strain and not exactly plane strain deformation conditions, as it is required by (14).

Under these circumstances, both integration of the damage functions along the strain loading paths and the approximate procedure based in Eq. (14) can be utilized to determine the critical values of damage at the onset of fracture. Fig. 6 presents the contour of the critical damage D^{crit} as a function of the major and minor in-plane strains obtained from a hole-flanged part made from a blank with a pre-cut hole diameter $D_0 = 102$ mm that failed by fracture at the second intermediate drawing angle $\psi_i = 70^{\circ}$. The contour of the critical damage D^{crit} at the onset of failure by cracking (Fig. 6) reveals an increase of approximately 8% against the maximum accumulated damage D^{max} that was found in

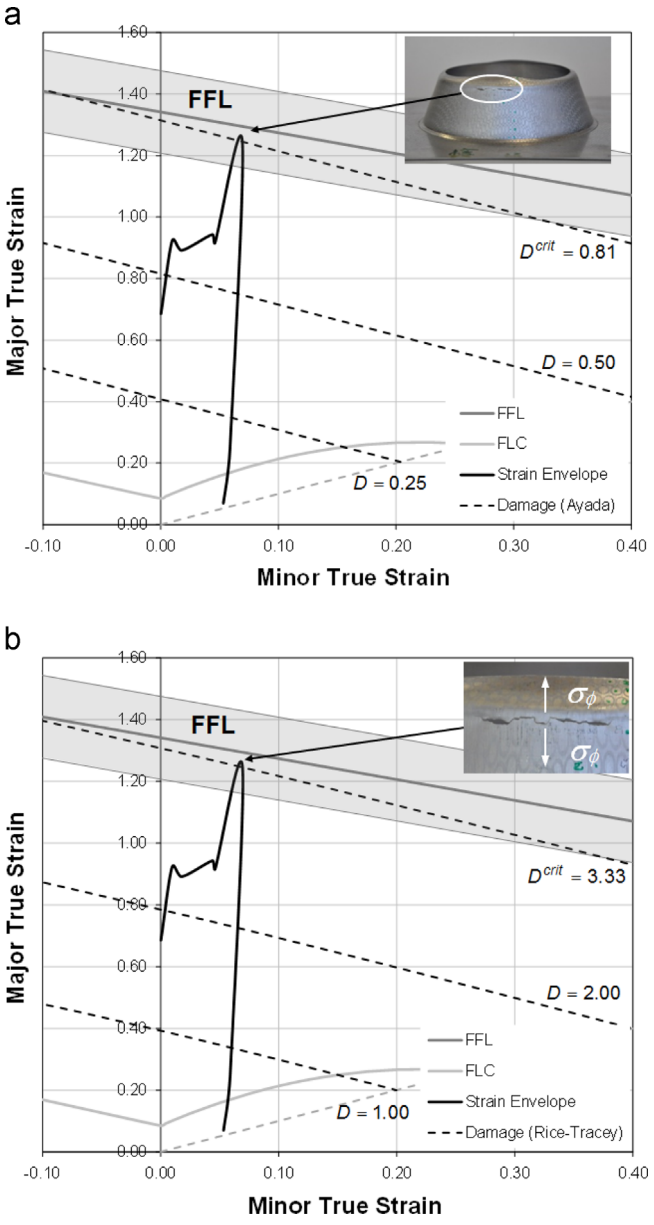

Fig. 6. Strain envelope in the principal strain space with line contours (black dashed lines) showing different values of accumulated damage D according to (a) Ayada et al. and (b) Rice and Tracey for a hole-flanged part made from a blank with a pre-cut hole diameter $D_0 = 102$ mm. The values of critical damage D^{crit} correspond to the onset of failure by cracking.

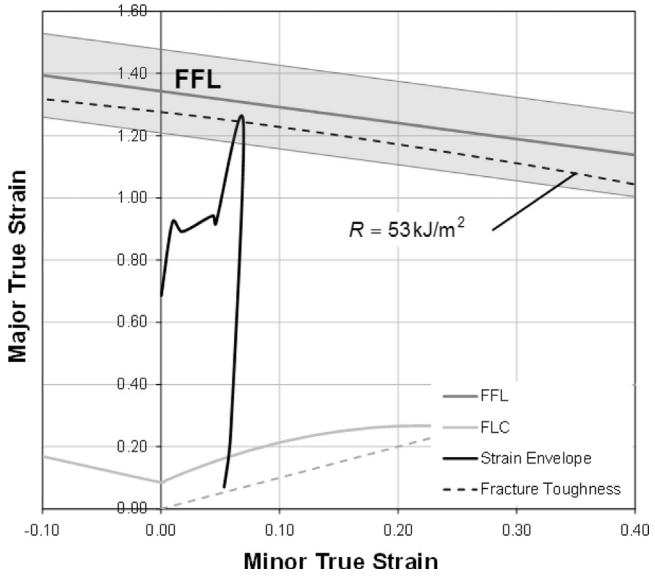

Fig. 7. Strain envelope in the principal strain space with the iso-contour of fracture toughness R (kJ/m^2) (refer to the black dashed line).

hole-flanged SPIF parts that were successfully made from blanks with a diameter $D_0=121$ mm (refer to Fig. 5).

The contour of the critical damage D^{crit} at the onset of failure by cracking (Fig. 6) also reveals an inclination slightly different from that of the FFL, which was independently determined by means of sheet formability tests covering strain paths from uniaxial to plane-strain and biaxial loading conditions (Fig. 2). The difference in inclination is the result of three pertinent assumptions of the proposed methodology. Firstly, ductile damage is not coupled. Secondly, Hill's 1948 criterion is not the best option for describing the anisotropic behavior of sheet metals with $r<1$, like aluminum AA1050-H111. However, other anisotropic yield criteria more suitable for describing the anisotropic behavior of aluminum would create mathematical difficulties in obtaining a closed-form analytical methodology for determining the accumulated values of ductile damage and fracture toughness from the experimental values of strain. Thirdly, there may be a threshold of strain $\bar{\varepsilon}_0$ below which ductile damage is not accumulated as claimed by Atkins and Mai [22]. This possibility requires integration of the accumulated values of damage in Eq. (10), as follows,

$$D_{Ayada}=\int_{\bar{\varepsilon}_0}^{\bar{\varepsilon}}\frac{\sigma_m}{\bar{\sigma}}d\bar{\varepsilon}$$

$$D_{Rice-Tracey}=\int_{\bar{\varepsilon}_0}^{\bar{\varepsilon}}\exp\left(\frac{3}{2}\times\frac{\sigma_m}{\bar{\sigma}}\right)d\bar{\varepsilon} \quad (15)$$

and would lead to changes in the inclination of the iso-accumulated contours of damage. In particular, it would provide an upward curvature of the iso-contours towards the FFL in the first quadrant of the principal strain space [24].

3.3. Fracture toughness

Following a similar procedure to that employed for the critical values of damage, it is possible to determine fracture toughness R by integrating the work of surface formation along the deformation history of material elements until failure by fracture (12) [22,25] or, alternatively, by means of the following expression solely based on the value of the effective strain $\bar{\varepsilon}_f$ at fracture,

$$R=t\int_0^{\bar{\varepsilon}_f}\bar{\sigma}\,d\bar{\varepsilon}=t\frac{K\varepsilon_f^{n+1}}{(n+1)} \quad (16)$$

In the above equation, material is assumed to follow a Ludwik–Hollomon's stress–strain equation $\bar{\sigma}=K\bar{\varepsilon}^n$ (1) and t is the actual thickness of the sheet.

The results provided by Eqs. (12) and (16) are identical and give $R=53$ kJ/m^2 (Fig. 7) because (16) does not include any assumption regarding plane strain loading conditions.

The value of R confirms the excellent ductility of AA1050-H111 and copes with the large distance from neck formation (FLC) to collapse by fracture (FFL), corresponding to a reduction in sheet thicknesses from below 40% to approximately 70%, that had been observed during the formability tests (refer to Fig. 2b).

The abovementioned results lead us to conclude that AA1050-H111 has a high ability to resist fracture by cracking. Moreover, the morphology of the cracks around the circumferential direction lead us further to conclude that fracture toughness R obtained from hole-flanging by SPIF is characterized under mode I crack opening because the failure mechanism appears to be the result of normal tensile meridional stresses perpendicular to the crack (refer to the photographs included in Fig. 6).

4. Conclusions

Critical ductile damage and fracture toughness of aluminum AA1050-H111 sheets were determined by means of a new methodology that combines circle grid analysis and plasticity theory with experimentation in hole-flanging by means of single point incremental forming (SPIF).

The methodology traces the strains and stresses of selected grid points corresponding to different regions of the sheet metal parts at various intermediate stages of deformation in order to accumulate the energy per unit of volume and the work of surface formation up to the onset of failure by fracture. Fracture toughness corresponds to crack opening mode I under normal tensile meridional stresses acting perpendicular to the crack.

A simplified procedure to determine the experimental values of critical ductile damage and fracture toughness that is exclusively based on the values of the effective strain at the onset of failure by fracture is also presented. The procedure allows quick and easy calibration but its utilization is limited to material flow under plane-strain (or near-plane strain) loading conditions. The overall methodology can be easily extended to other materials (e.g. polymers).

Acknowledgments

The work was partially supported by the Portuguese Foundation for Science and Technology under the research Contract PEst-OE/EME/LA0022/2011. Luciana Montanari would like also to acknowledge FAPESP (Fundação de Amparo à Pesquisa do Estado de São Paulo) for the financial support.

The work of André Teodora and Pedro Pardal is greatly acknowledged.

References

[1] Jeswiet J, Micari F, Hirt G, Bramley A, Duflou J, Allwood J. Asymmetric single point incremental forming of sheet metal. Ann CIRP 2005;54:623–50.
[2] Allwood J, Shouler DR, Tekkaya AE. The increased forming limits of incremental sheet forming processes. In: Proceedings of the international conference on sheet metal, SheMet '07, Palermo, Italy; 2007 p. 621–628.
[3] Eycken P, He S, van Bael A, van Houtte P, Duflou J. Forming limit predictions for the serrated strain paths in single point incremental sheet forming. In: Proceedings of the 9th international conference on numerical methods in industrial forming processes, NUMIFORM, Porto, Portugal; 2007, p. 141–146.
[4] Silva MB, Skjoedt M, Atkins AG, Bay N, Martins PAF. Single point incremental forming and formability/failure diagrams. J Strain Anal Eng Des 2008;43:15–36.

[5] Cao J., Huang Y., Reddy N.V., Malhotra R., Wang, Y. Incremental sheet metal forming: advances and challenges. In: Proceedings of the international conference on technology of plasticity, ICTP, Gyeongju. South Korea; 2008, p. 751–752.
[6] Jackson K, Allwood J. The mechanics of incremental sheet forming. J Mater Process Technol 2009;209:1158–74.
[7] Silva MB, Nielsen PS, Bay N, Martins PAF. Failure mechanisms in single-point incremental forming of metals. Int J Adv Manuf Technol 2011;56:893–903.
[8] Emmens WC, van den Boogaard AH. An overview of stabilizing deformation mechanisms in incremental sheet forming. J Mater Process Technol 2009;209:3688–95.
[9] Oyane M. Criteria for ductile fracture and their applications. J Mech Work Technol 1980;4:65–81.
[10] Huang Y, Cao J, Smith KS, Woody B, Ziegert J, Li M. Experimental and numerical investigation of forming limits in incremental forming of a conical cup. Trans N Am Manuf Res Inst SME 2008;36:389–96.
[11] Malhotra R, Xue L, Belytschko T, Cao J. Mechanics of fracture in single point incremental forming. J Mater Process Technol 2012;212:1573–90.
[12] Xue L. Damage accumulation and fracture initiation in uncracked ductile solids subjected to triaxial loading. Int J Solids Struct 2007;44:5163–81.
[13] Keeler SP. Circular Grid System – a valuable aid for evaluating sheet metal formability. SAE Technical Paper 680092; 1968.
[14] Goodwin G. Application of strain analysis to sheet metal forming problems in the press shop. SAE Technical Paper 680093; 1968.
[15] Glover G, Duncan JL, Embury JD. Failure maps for sheet metal. Met Technol 1977;4:153–9.
[16] Atkins AG. Fracture in forming. J Mater Process Technol 1996;56:609–18.
[17] Montanari L, Cristino VA, Silva MB, Martins PAF. A new approach for deformation history of material elements in hole-flanging produced by single point incremental forming. Int J Adv Manuf Technol 2013;69:1175–83.
[18] Hill R. A theory of yielding and plastic flow of anisotropic metals. Proc R Soc Lond (Ser A) 1948;193:281–97.
[19] Ayada M, Higashino T, Mori K. Central bursting in extrusion of inhomogeneous materials. Advanced technology of plasticity. In: Proceedings of the 2nd international conference on technology of plasticity, Stuttgart, Germany, vol. 1; 1987 p. 553–558.
[20] Rice JR, Tracey DM. On the ductile enlargement of voids in triaxial stress fields. J Mech Phys Solids 1969;17:201–17.
[21] Gouveia BPPA, Rodrigues JMC, Martins PAF. Fracture predicting in bulk metal forming. Int J Mech Sci 1996;38:361–72.
[22] Atkins AG, Mai YW. Elastic and plastic fracture: metals, polymers, ceramics, composites, biological materials. Chichester, UK: Ellis Horwood; 1985.
[23] Atkins AG, Mai YW. Fracture strains in sheet metal forming and specific essential work of fracture. Eng Fract Mech 1987;27:291–7.
[24] Atkins AG. Fracture mechanics and metalforming: damage mechanics and the local approach of yesterday and today. Fracture research in retrospect. Rotterdam, The Netherlands: AA Balkema; 1997; 327–50.
[25] Muscat-Fenech CM, Arndt S, Atkins AG. The determination of fracture forming limit diagrams from fracture toughness. In: Proceedings of the 4th international conference sheet metal 1996, University of Twente, The Netherlands, vol. 1; 1996, p. 249–260.